Topology and entanglement in quench dynamics

Po-Yao Chang*
Center for Materials Theory, Rutgers University, Piscataway, New Jersey 08854, USA

(Received 5 May 2018; published 11 June 2018)

We classify the topology of the quench dynamics by homotopy groups. A relation between the topological invariant of a postquench order parameter and the topological invariant of a static Hamiltonian is shown in $d+1$ dimensions ($d = 1,2,3$). The midgap states in the entanglement spectrum of the postquench states reveal their topological nature. When a trivial quantum state is under a sudden quench to a Chern insulator, the midgap states in the entanglement spectrum form rings. These rings are analogous to the boundary Fermi rings in the Hopf insulators. Finally, we show a postquench order parameter in 3+1 dimensions can be characterized by the second Chern number. The number of Dirac cones in the entanglement spectrum is equal to the second Chern number.

DOI: 10.1103/PhysRevB.97.224304

I. INTRODUCTION

Recently, properties of quantum states far from equilibrium attract huge attention due to the progressive developments in cold-atom experiments. For example, a quantum Newton's cradle setup is realized in one-dimensional Bose gases [1] and the emergence of quantum turbulence is observed in a Bose-Einstein condensate [2]. Besides examining the dynamical properties of nonequilibrium states, cold-atom experiments also provide a playground for engineering topological systems including the Su-Schrieffer-Heeger model [3], the Hofstadter model [4–6], and the Haldane model (Chern insulators) [7,8]. These topological phases are typically classified by the topological invariant in the static Hamiltonian. The classification of the topological phases out of equilibrium is one of the main interests in both condensed-matter and cold-atom communities.

To study nonequilibrium topological phases, one straightforward setup is Floquet systems. The band inversion mechanism is introduced by a periodically driven source and gives rise to a Floquet topological insulator [9–11]. Another setup is considering a dynamical process in which an initial state of a trivial Hamiltonian is evolved under a sudden quench to a nontrivial Hamiltonian. This quantum quench involves the change of the topological number and can be revealed in the postquench states. In a generic one-dimensional two-band model, a dynamic Chern number characterizes the topological property of the postquench state [12,13]. In a two-band Chern insulator, the dynamics of the postquench state can be captured by the Hopf number [14,15]. The postquench dynamics across a quantum critical point is also influenced by the topological edge states [16–20]. The topology of the static Hamiltonian and topology of the postquench state are related.

In this paper, we establish this relation in a systematic way by use of homotopy groups. We show that the postquench state is periodic in time under a sudden quench to a translational invariant Hamiltonian in d dimensions ($d = 1,2,3$). The momentum-time space is a $(d+1)$-dimensional torus T^{d+1}. A mapping from the time-momentum space T^{d+1} to a manifold $\mathcal{M}$ of the postquench order parameter is characterized by the homotopy group $\pi_{d+1}(\mathcal{M})$. In a two-band model, the manifold of the postquench pseudospin is a two-sphere S^2. Due to the nonvanishing homotopy groups $\pi_{1+1}(S^2)$ and $\pi_{2+1}(S^2)$, the postquench states have nontrivial topology in one and two dimensions. However, in a generic n-band model ($n > 2$), the postquench order parameter can be a higher-dimensional manifold $\mathcal{M} \neq S^2$. The statement for two-band models, in general, cannot generalize to n-band models ($n > 2$). We consider two different strategies to overcome this obstacle. First, we project both the static Hamiltonian and the postquench state in the submanifolds that have similar structures as a two-band model. We demonstrate this strategy by spin-1 models. Second, we consider higher-order homotopy groups to classify both the static Hamiltonian and the postquench order parameter. In a four-band model, we demonstrate the relation between the three-dimensional winding number of the static Hamiltonian [classified by $\pi_3(S^3)$] and the second Chern number of the postquench order parameter [classified by $\pi_4(S^4)$].

The entanglement spectrum also reveals the topological property of the postquench states. In $(1+1)$-dimensional postquench states, the entanglement spectrum has crossings when the dynamic Chern number of the postquench order parameter is nonzero [13]. Here, we extend this analysis to 2+1 and 3+1 dimensions and consider two different bipartitions. In a real-space bipartition, we show that when the postquench state is nontrivial, midgap states in the entanglement spectrum form Dirac cones in 2+1 and 3+1 dimensions. The number of Dirac cones in the entanglement spectrum directly links to the topological index of the postquench states. We compute the topological index of the postquench states and show it relates to the topological invariant of the postquench order parameters. In a frequency space bipartition [21], we show that the midgap states in the entanglement spectrum in 2+1 dimensions form rings. In this case, the topological invariant of the postquench order parameter is characterized by the Hopf number. These rings in the entanglement spectrum are analogous to the boundary Fermi rings in the Hopf insulators [22–24].

*pychang@physics.rutgers.edu

The rest of the paper is organized as follows: In Sec. II, we introduce the quench protocol and the classification scheme by homotopy groups. In Sec. III, we review the quench dynamics of two-band models and introduce a different quench process which has not been discussed before. In Sec. IV, we show the quench dynamics and the entanglement spectrum of the postquench states in spin-1 models. In Sec. V, we demonstrate that the second Chern number captures the quench dynamics in 3+1 dimensions in a four-band model. In Sec. VI, we conclude our work and provide some discussion.

II. QUENCH PROTOCOL

We consider a free-fermion Hamiltonian with discrete translational symmetries

$$H = \sum_{\mathbf{k}} \sum_{i,j,=1}^{n} c^{\dagger}_{\mathbf{k},i} \mathcal{H}^{ij}_{\mathbf{k}} c_{\mathbf{k},j}, \tag{1}$$

where $\mathbf{k}$ is the momentum, $\mathcal{H}^{ij}_{\mathbf{k}}$ is the single-particle Hamiltonian with n being the number of bands, and $c^{\dagger}_{\mathbf{k},i}$ is the fermionic operator in the momentum space. If the single-particle Hamiltonian $\mathcal{H}^{ij}_{\mathbf{k}}$ has a massive Dirac Hamiltonian representation, one can classify the possible distinctive Dirac mass term by homotopy groups [25–28]. This classification requires the number of bands to be large. On the other hand, in few-band models, the classification of the single-particle Hamiltonian can also be obtained from the structure of the single-particle Hamiltonian directly [22–24,29–31]. In particular, we can parametrize these few-band models with a finite set of functions $\{f_{\mathbf{k},\alpha}\}$. Each point in the momentum space (which is a d-dimensional torus) maps to a point in the manifold $\mathcal{M}$ of this set of functions. We can classify distinct sets of functions by the dth homotopy group $\pi_d(\mathcal{M})$.

The evolution operator of the many-body state is $\hat{U}(t) = e^{-iHt}$. Let us assume the initial many-body state $|\Psi_i\rangle$ is prepared from a given Hamiltonian H_i such that $|\Psi_i\rangle = \prod_{\mathbf{k},\alpha\in\text{occ.}} d^{\dagger}_{\mathbf{k},\alpha}|0\rangle$, with $d_{\mathbf{k},\alpha}$ being the fermionic operator in the energy basis of the initial Hamiltonian $H_i = \sum_{\mathbf{k},\alpha} \epsilon_{\mathbf{k},\alpha} d^{\dagger}_{\mathbf{k},\alpha} d_{\mathbf{k},\alpha}$, and "occ." refers to the occupied bands. Here $\epsilon_{\mathbf{k},\alpha}$ is the eigenenergy of H_i. The corresponding single-particle wave function is $d^{\dagger}_{\mathbf{k},\alpha}|0\rangle = \sum_i u_{\alpha,i} c^{\dagger}_{\mathbf{k},i}|0\rangle$, where $u_{\alpha,i}$ is the unitary matrix diagonalizing H_i.

The postquench many-body state is

$$\begin{aligned} |\Psi(t)\rangle &= \hat{U}(t)|\Psi_i\rangle \\ &= \prod_{\mathbf{k},\alpha} e^{-it\sum_{i,j} \mathcal{H}^{ij}_{\mathbf{k}} c^{\dagger}_{\mathbf{k},j} c_{\mathbf{k},j}} d^{\dagger}_{\mathbf{k},\alpha}|0\rangle \\ &= \prod_{\mathbf{k},\alpha} \sum_{i,j} [e^{-it\mathcal{H}_{\mathbf{k}}}]_{ij} u_{\alpha,j} c^{\dagger}_{\mathbf{k},i}|0\rangle, \end{aligned} \tag{2}$$

which is factorized in the momentum $\mathbf{k}$. Hence we only need to focus on the single-particle evolution operator $U_{\mathbf{k}}(t) = e^{-it\mathcal{H}_k}$ acting on the single-particle wave function, i.e., particles do not interchange the momentum due to its noninteracting nature. We can consider a measure of an operator $\mathbf{O}_{\mathbf{k}} = \sum_{i,j} c^{\dagger}_i \mathcal{O}^{ij}_{\mathbf{k}} c_j$ by the postquench state, $\langle \mathbf{O}_{\mathbf{k}}(t)\rangle = \langle \Psi(t)|\mathbf{O}_{\mathbf{k}}|\Psi(t)\rangle = \sum_{\alpha,\beta,\gamma} [e^{it\mathcal{H}_{\mathbf{k}}}]_{\alpha\beta} \mathcal{O}^{\beta\gamma}_{\mathbf{k}} [e^{-it\mathcal{H}_{\mathbf{k}}}]_{\gamma\alpha}$, where $\mathcal{O}^{\beta\gamma}_{\mathbf{k}} = u^{\dagger}_{\beta i} \mathcal{O}^{ij}_{\mathbf{k}} u_{\gamma j}$. This postquench measurement defines an order parameter $\langle \mathbf{O}_{\mathbf{k}}(t)\rangle$ on a manifold $\mathcal{M}'$.

For a finite system, the postquench state will recur to its initial state. The momentum-time space is a $d+1$ torus, and we can consider a mapping from a point in this $d+1$ torus to a point in the order parameter space $\mathcal{M}'$. We can classify distinct sets of the order parameter space by the $(d+1)$th homotopy group $\pi_{d+1}(\mathcal{M}')$.

We demonstrate few examples where the classification of the postquench order parameter $\pi_{d+1}(\mathcal{M}')$ had direct relation to the classification of the static Hamiltonian $\pi_d(\mathcal{M})$ in $d = 1,2,3$ dimensions and n-band models with $n = 2,3,4$.

III. TWO-BAND MODELS

A generic two-band Hamiltonian can be written as $\mathcal{H}_{\mathbf{k}} = a_{\mathbf{k}} \mathbb{I}_{2\times 2} + (f_{\mathbf{k}}, g_{\mathbf{k}}, h_{\mathbf{k}}) \cdot \boldsymbol{\sigma}$, where $\boldsymbol{\sigma} = (\sigma_x, \sigma_y, \sigma_z)$ are the Pauli matrices. The corresponding energy is $E_{\mathbf{k}} = a_{\mathbf{k}} \pm \sqrt{f^2_{\mathbf{k}} + g^2_{\mathbf{k}} + h^2_{\mathbf{k}}}$. Since $a_{\mathbf{k}}$ just shifts the energy, the topology of the Hamiltonian is independent of $a_{\mathbf{k}}$. For simplicity, we remove $a_{\mathbf{k}}$ in the following discussion.

In one-dimensional cases, we consider a symmetry constraint restricting the Hamiltonian such that one of the Pauli matrices is forbidden. For example, a chiral symmetry constrains the Hamiltonian $\mathcal{S} :\to \mathcal{S}^{\dagger}\mathcal{H}_k\mathcal{S} = -\mathcal{H}_k$. Then $h_k = 0$ if $\mathcal{S} = \sigma_z$. The manifold of the Hamiltonian can be seen as a ring with the parametrization $e^{i\theta_k} = \frac{f_k + ig_k}{\sqrt{f_k^2 + g_k^2}}$. The classification for a point in k to θ_k is given by the first homotopy group $\pi_1(S^1) = \mathbb{Z}$ and can be indexed by the winding number

$$\begin{aligned} \nu &= \frac{1}{2\pi} \int dk \frac{d\theta_k}{dk} \\ &= \frac{1}{2\pi} \int dk \frac{1}{f_k^2 + g_k^2} [f_k \partial_k g_k - g_k \partial_k f_k]. \end{aligned} \tag{3}$$

In two-dimensional cases, we do not consider any symmetry constraints. All the components $(f_{\mathbf{k}}, g_{\mathbf{k}}, h_{\mathbf{k}})$ are nonvanishing. The manifold of the Hamiltonian is a two-sphere where we can parametrize it by a unit vector $\hat{d}_{\mathbf{k}} = \frac{(f_{\mathbf{k}}, g_{\mathbf{k}}, h_{\mathbf{k}})}{\sqrt{f^2_{\mathbf{k}} + g^2_{\mathbf{k}} + h^2_{\mathbf{k}}}}$. The second homotopy group classifies the Hamiltonian by $\pi_2(S^2) = \mathbb{Z}$ and can be indexed by the Chern number

$$C = \frac{1}{4\pi} \int d^2k \hat{d}_{\mathbf{k}} \cdot \left[\partial_{k_x} \hat{d}_{\mathbf{k}} \times \partial_{k_y} \hat{d}_{\mathbf{k}}\right]. \tag{4}$$

Now we consider an initial state $|\psi_i\rangle$ which evolves under the evolution operator $U_{\mathbf{k}}(t) = e^{-i\mathcal{H}_{\mathbf{k}}t}$, $|\psi_{\mathbf{k}}(t)\rangle = U_{\mathbf{k}}(t)|\psi_i\rangle$. The evolution operator can be written as $U_{\mathbf{k}}(t) = \cos(|E_{\mathbf{k}}|t) - i\mathcal{H}_{\mathbf{k}} \sin(|E_{\mathbf{k}}|t)$. The postquench state will recur to its initial state at $t = 2\pi/|E_{\mathbf{k}}|$. Momentum and time $(\mathbf{k},t)$ form a $(d+1)$-dimensional torus, where d is the dimensions of the momentum space.

A. 1+1 dimensions

We first discuss the case when the static Hamiltonian $\mathcal{H}_k$ is in one dimension and the postquench state $|\psi_k(t)\rangle$ is in 1+1 dimensions. A pseudospin can be defined by the postquench state as $\hat{n}_k(t) = \langle \psi_k(t)|\boldsymbol{\sigma}|\psi_k(t)\rangle$. There are two possible scenarios for the postquench pseudospin. One scenario is that there

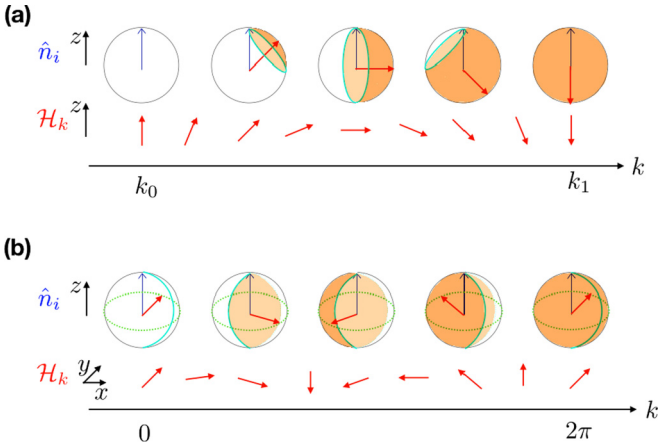

FIG. 1. An illustration of the topological relation between the nonvanishing winding number of the static Hamiltonian and the nonvanishing dynamic Chern number of the postquench pseudospin. The blue arrows correspond to the pseudospin of the initial state. The red arrows correspond to the directions of the pseudomagnetic field (Hamiltonian $\mathcal{H}_{\mathbf{k}}$). The light-blue (semi-)rings correspond to the trajectories of the pseudospin precession. (a) When there are two fixed points k_0 and k_1, the trajectories of the pseudospin precession wraps the Bloch sphere from k_0 to k_1 (shaded by orange). (b) When pseudospin of the initial state is perpendicular to the directions of the pseudomagnetic field, the trajectories of the pseudospin precession with a half period wraps the Bloch sphere from 0 to 2π (shaded by orange). Dashed green line shows the equator in the x-y plane.

can exist fixed points such that the postquench pseudospin is parallel or antiparallel to the pseudomagnetic field (static Hamiltonian $\mathcal{H}_{\mathbf{k}}$). The topological invariant characterizing the postquench pseudospin in this scenario is the dynamical Chern number [12,13],

$$C_{\text{dyn.}} = \frac{1}{4\pi}\int_{k_m}^{k_{m+1}} dk \int_0^{\pi} dt \hat{n}_k(t)\cdot[\partial_k \hat{n}_k(t)\times\partial_t \hat{n}_k(t)], \quad (5)$$

where k_m and k_{m+1} are two nearby fixed points in one-dimensional momentum space. It has been shown in Refs. [12,13] that the dynamic Chern number $C_{\text{dyn.}} = \pm 1$ if the winding number ν_i for the Hamiltonian of the initial state is different than the winding number ν of the Hamiltonian $\mathcal{H}_{\mathbf{k}}$, $\nu_i \neq \nu$. Pictorially, one can visualize this dynamical Chern number by monitoring how many times the trajectory of the postquench pseudospin wraps the Bloch sphere. We demonstrate this wrapping in Fig. 1(a). For a given k, the postquench pseudospin precesses along the direction of the pseudomagnetic field $d_k = (f_k, g_k, 0)$ with a circular trajectory on the Bloch sphere. If the static Hamiltonian $\mathcal{H}_{\mathbf{k}}$ has a nontrivial winding, the circular trajectory of the post-quench pseudospin can wrap the entire Bloch sphere from k_0 to k_1, where $k_{0(1)}$ is the fixed point with the postquench pseudospin (anti-)parallel to the pseudospin of the initial state.

Next, we consider the second scenario which has not been discussed before. This scenario has no fixed points for the postquench pseudospin. In general, the circular trajectories on the Bloch sphere of the postquench pseudospin from $k = 0$ to $k = 2\pi$ do not wrap the entire Bloch sphere. Here $k \in [0, 2\pi]$ is the Brillouin zone (BZ). However, when the pseudospin of the initial state is perpendicular to the direction of the pseudomagnetic field, the circular trajectories on the Bloch sphere of the postquench pseudospin from $k = 0$ to $k = 2\pi$ can wrap the entire Bloch sphere [see Fig. 1(b)].

Without loss of generality, we consider the static Hamiltonian $\mathcal{H}_{\mathbf{k}} = \hat{f}_{\mathbf{k}}\sigma_x + \hat{g}_{\mathbf{k}}\sigma_y$ and the initial state $|\psi_i\rangle = (1,0)^{\mathrm{T}}$. Here we normalize the static Hamiltonian $\hat{f}_{\mathbf{k}}^2 + \hat{g}_{\mathbf{k}}^2 = 1$. The postquench state is $|\psi_{\mathbf{k}}(t)\rangle = [\cos t, -i(\hat{f}_{\mathbf{k}} + i\hat{g}_{\mathbf{k}})\sin t]^{\mathrm{T}}$ and the postquench pseudospin is $\hat{n}_{\mathbf{k}}(t) = (\hat{g}_{\mathbf{k}}\sin 2t, \hat{f}_{\mathbf{k}}\sin 2t, \cos 2t)$. Since there is no fixed point, we need to integrate out the entire momentum space for the corresponding dynamical Chern number, which is defined as

$$\begin{aligned} C'_{\text{dyn.}} &= \frac{1}{4\pi}\int_0^{2\pi} dk \int_0^{\pi/2} dt \hat{n}_{\mathbf{k}}(t)\cdot[\partial_k \hat{n}_{\mathbf{k}}(t)\times\partial_t \hat{n}_{\mathbf{k}}(t)] \\ &= \frac{-1}{2\pi}\int_0^{\pi/2} \sin 2t \int_0^{2\pi} dk[f_k\partial_k g_k - g_k\partial_k f_k] \\ &= -\nu. \end{aligned} \quad (6)$$

Because of the intrinsic symmetry, $\hat{n}_{\mathbf{k}}(t)\cdot[\partial_k \hat{n}_{\mathbf{k}}(t)\times\partial_t \hat{n}_{\mathbf{k}}(t)] = \hat{n}_{\mathbf{k}}(-t)\cdot[\partial_k \hat{n}_{\mathbf{k}}(-t)\times\partial_t \hat{n}_{\mathbf{k}}(-t)]$, we integrate half of the period (0 to $\pi/2$) of the postquench pseudospin to have the nonvanishing dynamical Chern number. Figure 1(b) shows how the trajectories of the pseudospin precess with half period wraps the Bloch sphere when there is a nonvanishing winding number of the static Hamiltonian $\mathcal{H}_{\mathbf{k}}$.

To demonstrate the topological property of the postquench states, we consider the Su-Schrieffer-Heeger model, where $f_k = t_1 + t_2\cos k$ and $g_k = t_2\sin k$. When $|t_1/t_2| < 1$ the winding number $\nu = 1$ and $|t_1/t_2| > 1$ the winding number $\nu = 0$. One way to characterize topological property of the postquench states is the entanglement spectrum. One can consider a spatial bipartition (A and B subsystems) and construct the reduced density matrix $\rho_A(t) = \mathrm{Tr}_B|\Psi(t)\rangle\langle\Psi(t)| = \mathcal{N}^{-1}e^{-H_A(t)}$, where $H_A(t)$ is the entanglement Hamiltonian and $\mathcal{N}$ is the normalization condition such that $\mathrm{Tr}_A\rho_A(t) = 1$. In free-fermion systems, the spectrum of the entanglement Hamiltonian can be directly extracted from the correlation matrix $C^A_{x,x'}(t) = \langle\Psi(t)|c_x^\dagger c_{x'}|\Psi(t)\rangle$, with x, x' in the subsystem A [32,33]. The entanglement spectrum $\xi(t)$ is the defined as the eigenvalue of the reduced density matrix $C^A_{x,x'}(t)$. In the first scenario where there are fixed points, it is shown in Ref. [13] that the entanglement spectrum has crossings if the dynamic Chern number is nonvanishing. Here, we demonstrate that in the second scenario, the entanglement spectrum also has crossings if the dynamic Chern number is nonvanishing. Figure 2(a) shows when $t_1/t_2 = 0.5$, the midgap states in the entanglement spectrums cross. These midgap states are localized at the entanglement boundary. This is the bulk boundary correspondence in the entanglement Hamiltonian. If the dynamic Chern number is nonvanishing, there are robust boundary modes in the entanglement Hamiltonian. On the other hand, if the dynamic Chern number is zero, there are no localized midgap states, as shown in Fig. 2(b).

In two-band models, the postquench pseudospin $\hat{n}_{\mathbf{k}}(t)$ contains the same information as the postquench projector $P_k(t) = |\psi_k\rangle\langle\psi_k| = \frac{1}{2}[1 + \tilde{n}_k(t)\cdot\boldsymbol{\sigma}]$, where $\tilde{n}_k(t) = (\hat{g}_k\sin 2t, -\hat{f}_k\sin 2t, \cos 2t)$. Hence the topological invariant computed from the postquench pseudospin can reflect the

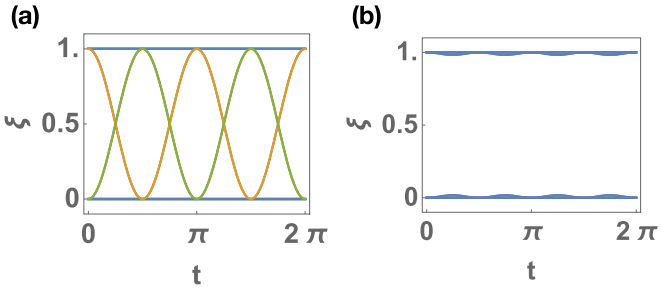

FIG. 2. Entanglement spectrum $\xi(t)$ for a real-space bipartition with (a) $t_1/t_2 = 0.5$. The green (orange) line indicates the corresponding eigenstate localized at the left (right) entangling boundary between subsystems A and B. (b) $t_1/t_2 = 2$. There are no crossings in the entanglement spectrum.

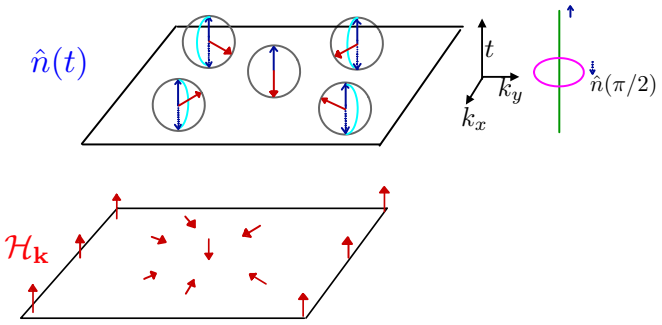

FIG. 3. An illustration of the topological relation between nonvanishing Chern number of the static Hamiltonian and the nonvanishing Hopf number of the postquench pseudospin. The blue arrows correspond to the pseudospin $\hat{n}_\mathbf{k}(t)$ of the initial state [upper panel]. The red arrows correspond to the direction of the pseudomagnetic field $d_\mathbf{k} = (f_\mathbf{k}, g_\mathbf{k}, h_\mathbf{k})$ [lower panel]. The light-blue arcs correspond to the trajectories of the pseudospin $\hat{n}_\mathbf{k}(t)$ precession from $t = 0$ to $\pi/2$ [upper panel]. The dashed blue arrows are the pseudospin at $t = \pi/2$ [upper panel]. In the upper-right panel, the green line corresponds to the inverse mapping from the pseudospin pointing to the north pole at center to the momentum-time space. The pink ring corresponds to the inverse mapping from the pseudospin pointing to the south pole at $t = \pi/2$ to the momentum-time space. The green line and the pink ring form a Hopf link that relates to the nonvanishing Hopf number of the postquench pseudospin.

topology of the postquench state and can reveal its property in the entanglement spectrum. In $(1+1)$-dimensional cases, the Chern number C computed from the postquench state is $C = -C'_{\text{dyn.}} = \nu$. This indicates that the number of crossings of the midgap states in the entanglement Hamiltonian is related to the dynamical Chern number of the postquench order parameter. Since the dynamical Chern number is computed from $t = 0$ to $t = \pi/2$, the number of crossings in the entanglement spectrum in the region $t \in [0,\pi/2]$ equals the dynamical Chern number due to the bulk boundary correspondence.

B. 2+1 dimensions

For the case that the static Hamiltonian is in two dimensions and the postquench state is in 2+1 dimensions, the postquench pseudospin is defined as $\hat{n}_\mathbf{k}(t) = \langle\psi_\mathbf{k}(t)|\boldsymbol{\sigma}|\psi_\mathbf{k}(t)\rangle$ on the Bloch sphere. One can consider a mapping from (t,k_x,k_y) to $\hat{n}_k$ that can be classified by the third homotopy group $\pi_3(S^2)$. The topological index is characterized by the Hopf number [34]

$$\chi = \int d^2k dt \mathbf{F}_\mathbf{k}(\mathbf{t}) \cdot \mathbf{A}_\mathbf{k}(\mathbf{t}), \tag{7}$$

where $F^i_\mathbf{k}(t) = \frac{1}{8\pi}\epsilon^{ijk}\hat{n}_\mathbf{k}(t)\cdot[\partial_j\hat{n}_\mathbf{k}(t)\times\partial_k\hat{n}_\mathbf{k}(t)]$ and $A^i_\mathbf{k}(t)$ is the Berry connection satisfying $F^i_\mathbf{k}(t) = \epsilon^{ijk}\partial_j A^k_\mathbf{k}(t)$. In a two-band model, the Berry connection $A^i_\mathbf{k}(t)$ and Berry flux $F^i_\mathbf{k}(t)$ can be computed from the postquench state $A^i_\mathbf{k}(t) = i\langle\psi_\mathbf{k}(t)|\partial_i\psi_\mathbf{k}(t)\rangle$ and $F^i_\mathbf{k}(t) = \frac{1}{2\pi}\epsilon^{ijk}\langle\partial_j\psi_\mathbf{k}(t)|\partial_k\psi_\mathbf{k}(t)\rangle$. It has been shown in Refs. [14,15] that the Hopf number is nonvanishing if the Chern number of the static Hamiltonian is nonzero.

The relation between the nonvanishing Chern number of the static Hamiltonian and the nonvanishing Hopf number is illustrated in Fig. 3. If the static Hamiltonian has a nonvanishing Chern number, the direction of the pseudomagnetic field $d_\mathbf{k} = (f_\mathbf{k}, g_\mathbf{k}, h_\mathbf{k})$ forms a skyrmion texture. The postquench pseudospin precesses under the pseudomagnetic field. For a given direction of the pseudospin, there is an inverse mapping from $\hat{n}_\mathbf{k}(t) \to (k_x,k_y,t)$ such that the trajectory in the momentum-time space is a closed loop. If the postquench pseudospin has a nonvanishing Hopf number, the inverse mapping of two different pseudospins forms a Hopf link in the momentum-time space [14,15]. As demonstrated in Fig. 3, the pseudospin at center is antiparallel to the pseudomagnetic field and does not precess. The inverse mapping is a line along the t axis. For the pseudospins perpendicular to the pseudomagnetic fields which are pointing to the center, these pseudospins will precess to the south pole at $t = \pi/2$. The inverse mapping of these pseudospins pointing to the south pole is a ring at the $t = \pi/2$ plane encircling the inverse mapping of the pseudospins pointing along the north pole. These two trajectories in the momentum-time space form a Hopf link that relates to a nonvanishing Hopf number of the postquench pseudospin.

Now we will show the relation of the entanglement spectrum of the postquench state and its corresponding Hopf number characterizing the postquench pseudospin. To be specific, we consider the Hamiltonian with $f_\mathbf{k} = t_1 \sin k_x$, $g_\mathbf{k} = t_1 \sin k_y$, and $h_\mathbf{k} = M + \cos k_x + \cos k_y$.

The Chern number of this static Hamiltonian is $|C| = 1$ when $0 < |M/t_1| < 2$ and $C = 0$ otherwise. We consider the entanglement spectrum of the postquench state evolved from $|\psi_i\rangle = (1,0)^\mathrm{T}$. For simplicity, we flatten the Hamiltonian $|E_k| = 1$ such that the period of the postquench state is 2π. For a real-space bipartition, the entanglement spectrum has no crossings if the Hopf number is zero [Fig. 4(a)] and has two cones when the Hopf number $|\chi| = 1$ [Fig. 4(b)]. On the other hand, we can also consider a frequency space bipartition. The postquench state in the frequency space is $\psi_\mathbf{k}(\omega) = \int_0^{2\pi} dt e^{i\omega t}\psi_\mathbf{k}(t)$, with $\omega \in [0,1]$. The frequency space bipartition we considered is that $A : \omega \in [0,0.5]$ and $B : \omega \in [0.5,1]$. The entanglement spectrum has no crossing if the Hopf number is zero [Fig. 4(c)]. For the case Hopf number $|\chi| = 1$, the midgap states in the entanglement spectrum form a ring [Fig. 4(d)]. This ring in the entanglement spectrum is similar to the boundary Fermi ring in the Hopf insulators [22–24].

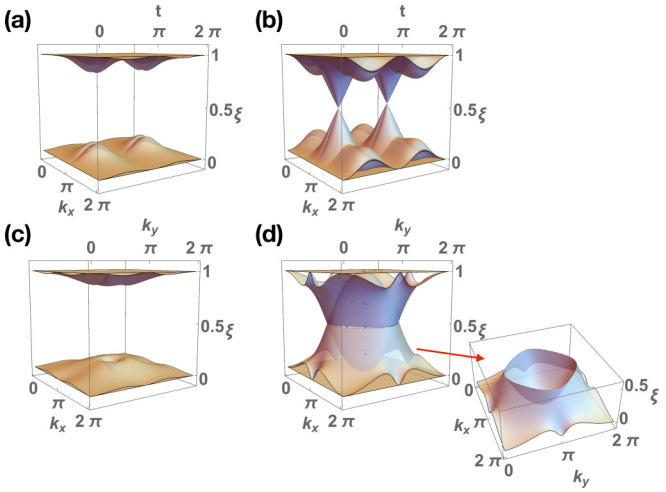

FIG. 4. Entanglement spectrum $\xi(k_x,t)$ for a real-space bipartition with (a) $(t_1,M)=(1,2.5)$, (b) $(t_1,M)=(1,0.5)$. Entanglement spectrum $\xi(k_x,k_y)$ for a frequency space bipartition with (c) $(t_1,M)=(1,2.5)$, (d) $(t_1,M)=(1,0.5)$. The right panel in (d) shows the midgap states form a ring.

Up to now, the relation between the Hopf number and the number of boundary Fermi rings in the Hopf insulators has not been established in the literature. It has been roughly discussed in Ref. [24] that there are more surfaces states when the absolute value of the Hopf number becomes larger. One should notice that in the Hopf insulators, all the Chern numbers computed from the three two-dimensional tori embedded in T^3 are zero. This indicates that there are no chiral modes on three boundaries due to vanishing Chern numbers in three directions. However, nonvanishing Hopf numbers generate gapless boundary states from the bulk boundary correspondence. Heuristically, the Fermi ring can be understood from a skyrmion texture of the pseudospin $\hat{n}(t)$ in the (k_r,t) plane, where $k_r=\sqrt{k_x^2+k_y^2}$. In Fig. 3, at $k_r=0$ and $k_r=k_{\text{boundary}}$, the pseudospin always points to the north pole. The trajectory in the momentum-time space where the pseudospin points to the south pole forms a ring [pink ring in Fig. 3]. Hence for a fixed $\theta_k=\tan^{-1}k_x/k_y$, the pseudospin $\hat{n}(t)$ has a space-time skyrmion texture in the (k_r,t) plane and leads to one chiral boundary mode in the entanglement Hamiltonian for a frequency space bipartition. The Fermi ring in the entanglement Hamiltonian is the collection of the chiral boundary modes from $\theta_k=0$ to 2π.

IV. THREE-BAND MODELS: SPIN-1 MODELS

A generic three-band model can be written as $\mathcal{H}_{\mathbf{k}}=a_{\mathbf{k}}\mathbb{I}_{3\times3}+\mathbf{b}_{\mathbf{k}}\cdot\boldsymbol{\lambda}$, where $\lambda_i, i=1,\ldots 8$ are Gell-Mann matrices spanning the Lie algebra of the SU(3) in the defining representation. We remove $a_{\mathbf{k}}$ in the Hamiltonian since it just shifts the energy level. One can flatten the Hamiltonian by using the eigenstate projectors in terms of Gell-Mann matrices as [35,36]

$$P_{\mathbf{k},\alpha}=|\psi_{\mathbf{k},\alpha}\rangle\langle\psi_{\mathbf{k},\alpha}|=\tfrac{1}{3}(1+\sqrt{3}\mathbf{n}_{\mathbf{k},\alpha}\cdot\boldsymbol{\lambda}), \tag{8}$$

where two conditions $\mathrm{Tr}\,P_{\mathbf{k},\alpha}=1$ and $P_{\mathbf{k},\alpha}^2=P_{\mathbf{k},\alpha}$ constrain the $\mathbf{n}_{\mathbf{k},\alpha}$ vectors to be a unit vector on S^7. The $\mathbf{n}_{\mathbf{k}}$ vector describes the manifold of the static Hamiltonian with higher dimension than S^1 and S^2. The homotopy group is zero in one and two dimensions, $\pi_1(S^7)=0$ and $\pi_2(S^7)=0$. To have the nontrivial homotopy group, we need to constrain the Hamiltonian to have the spin-1 structure, $\mathcal{H}_{\mathbf{k}}=\mathbf{d}_{\mathbf{k}}\cdot\mathbf{S}$, where $\mathbf{d}_{\mathbf{k}}=(f_{\mathbf{k}},g_{\mathbf{k}},h_{\mathbf{k}})$ and $\mathbf{S}=(S_x,S_y,S_z)$ are chosen from the linear combination of the Gell-Mann which satisfy the SU(2) subalgebra. In the following discussion, we consider the representation of $\mathbf{S}$ to be

$$S_x=\frac{1}{\sqrt{2}}\begin{pmatrix}0&1&0\\1&0&1\\0&1&0\end{pmatrix},\quad S_y=\frac{1}{\sqrt{2}}\begin{pmatrix}0&-i&0\\i&0&-i\\0&i&0\end{pmatrix},$$
$$S_z=\begin{pmatrix}1&0&0\\0&0&0\\0&0&-1\end{pmatrix}. \tag{9}$$

The corresponding energies are $E_0=0$ and $E_{\mathbf{k},\pm}=\pm\sqrt{f_{\mathbf{k}}^2+g_{\mathbf{k}}^2+h_{\mathbf{k}}^2}$.

The spin-1 models have the same classifications of static Hamiltonian as two-band models. In one-dimensional cases, if we eliminate one of the S_i (e.g., we set $h_{\mathbf{k}}=0$) in the Hamiltonian, the Hamiltonian can be classified by the first homotopy group $\pi_1(S^1)$ with the winding number $\nu=\frac{1}{2\pi}\int dk[\hat{f}_k\partial_k\hat{g}_k-\hat{g}_k\partial_k\hat{f}_k]$, where $\hat{f}_k=\frac{f_k}{\sqrt{f_k^2+g_k^2}}$ and $\hat{g}_k=\frac{g_k}{\sqrt{f_k^2+g_k^2}}$. In two-dimensional cases, we assume all the components in $\mathbf{d}_{\mathbf{k}}$ are nonvanishing. The Hamiltonian can be classified by the second homotopy group $\pi_2(S^2)$ with the Chern number $C=\frac{1}{4\pi}\int d^2k\hat{d}_{\mathbf{k}}\cdot[\partial_{k_x}\hat{d}_{\mathbf{k}}\times\partial_{k_y}\hat{d}_{\mathbf{k}}]$, where $\hat{d}_{\mathbf{k}}=\frac{\mathbf{d}_{\mathbf{k}}}{|\mathbf{d}_{\mathbf{k}}|}$.

The evolution operator of the spin-1 models satisfies the Rodrigues rotation formula [37],

$$\begin{aligned}U_{\mathbf{k}}(t)&=\exp[-i\mathcal{H}_{\mathbf{k}}t]\\&=\mathbb{I}_{3\times3}-i\mathcal{H}_{\mathbf{k}}\sin(|E_{\mathbf{k},\pm}|t)+\mathcal{H}_{\mathbf{k}}^2[\cos(|E_{\mathbf{k},\pm}|t)-1].\end{aligned} \tag{10}$$

We have $U_{\mathbf{k}}(2\pi/|E_{\mathbf{k},\pm}|)=U_{\mathbf{k}}(0)$. The postquench state will recur to the initial state at $t=2\pi/|E_{\mathbf{k},\pm}|$.

Here we define the postquench pseudospin $\hat{s}_{\mathbf{k}}=\langle\psi_{\mathbf{k}}(t)|\mathbf{S}|\psi_{\mathbf{k}}(t)\rangle$. Unlike two-band models, the postquench pseudospin in the spin-1 models is not guaranteed to be a unit vector. For example, $\hat{s}=\langle010|\mathbf{S}|010\rangle=(0,0,0)$ is a null vector, where (010) is a shorthand notation for a three-dimensional state $|\psi\rangle=(0,1,0)^{\mathrm{T}}$. We need to restrict the initial state such that the postquench pseudospin is a unit vector. In the representation of the $\mathbf{S}$ we chose, the initial state can be either $|\psi_i\rangle=(1,0,0)^{\mathrm{T}}$ or $(0,0,1)^{\mathrm{T}}$ to maintain the norm of the postquench pseudospin to be 1.

To summarize, in order to have nontrivial topology of both the static Hamiltonian and postquench order parameter in a three-band model, we focus on spin-1 models with a given initial state either $|\psi_i\rangle=(1,0,0)^{\mathrm{T}}$ or $(0,0,1)^{\mathrm{T}}$.

A. 1+1 dimensions

In 1+1 dimensional cases, we consider the static Hamiltonian $\mathcal{H}_k=f_kS_x+g_kS_y$ such that the topology of the static Hamiltonian can be indexed by the winder number ν. Let us

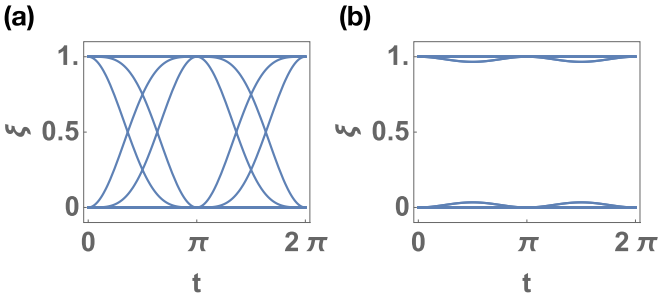

FIG. 5. Entanglement spectrum $\xi(t)$ computed from the postquench state defined in Eq. (11) for a real-space bipartition with (a) $(t_1,t_2)=(0.5,1)$ and (b) $(t_1,t_2)=(1,0.5)$.

assume the initial state is $|\psi_i\rangle=(1,0,0)^{\mathrm{T}}$. To further simplify the calculation and have a more compact form, we normalize the Hamiltonian $\hat{f}_k^2+\hat{g}_k^2=1$. The postquench state evolved under the evolution operator from Eq. (10) is

$$|\psi_k(t)\rangle=U_k(t)|\psi_i\rangle=\begin{pmatrix}\cos^2\frac{t}{2}(\hat{f}_k-i\hat{g}_k)\\ -i\sin t/\sqrt{2}\\ -\sin^2\frac{t}{2}(\hat{f}_k+i\hat{g}_k)\end{pmatrix}. \tag{11}$$

The postquench pseudospin is $\hat{s}(k,t)=(g_k\sin t,-f_k\sin t,\cos t)$ pointing on a two-sphere S^2. We can now define the dynamical Chern number characterizing the topology of the postquench pseudospin as

$$\begin{aligned}C'_{\mathrm{dyn.}}&=\frac{1}{4\pi}\int_0^{2\pi}dk\int_0^{\pi}dt\hat{s}\cdot(\partial_k\hat{s}\times\partial_t\hat{s})\\&=\frac{1}{4\pi}\int_0^{\pi}dt\sin t\int_0^{2\pi}dk[f_k\partial_k g_k-g_k\partial_k f_k]\\&=\nu.\end{aligned} \tag{12}$$

Similar to the two-band cases, there is an intrinsic symmetry such that $\hat{n}_{\mathbf{k}}(t)\cdot[\partial_k\hat{n}_{\mathbf{k}}(t)\times\partial_t\hat{n}_{\mathbf{k}}(t)]=\hat{n}_{\mathbf{k}}(-t)\cdot[\partial_k\hat{n}_{\mathbf{k}}(-t)\times\partial_t\hat{n}_{\mathbf{k}}(-t)]$. We integrate half of the period (0 to π) to have the nonvanishing dynamical Chern number.

In the case $\hat{f}_k=\frac{t_1+t_2\cos k}{\sqrt{(t_1+t_2\cos k)^2+t_2^2\sin^2 k}}$ and $\hat{g}_k=\frac{t_2\sin k}{\sqrt{(t_1+t_2\cos k)^2+t_2^2\sin^2 k}}$, we have $C'_{\mathrm{dyn.}}=\nu=1$ when $|t_1/t_2|<1$ and $C'_{\mathrm{dyn.}}=\nu=0$ when $|t_1/t_2|>1$. We can also computed the Chern number of the postquench state [Eq. (11)] directly,

$$\begin{aligned}C&=\frac{1}{2\pi i}\int_0^{2\pi}dk\int_0^{\pi}dt\langle\partial_t\psi_k(t)|\partial_k\psi_k(t)\rangle-\langle\partial_k\psi_k(t)|\partial_t\psi_k(t)\rangle\\&=\frac{1}{2\pi}\int_0^{\pi}dt\sin t\int_0^{2\pi}dk[f_k\partial_k g_k-g_k\partial_k f_k]\\&=2C'_{\mathrm{dyn.}}.\end{aligned} \tag{13}$$

The number of crossings of the midgap states in the entanglement Hamiltonian is direct related to the (dynamical) Chern number. Since the (dynamical) Chern number is computed from $t=0$ to $t=\pi$, the number of crossings in the entanglement spectrum in the region $t\in[0,\pi]$ equals the Chern number due to the bulk boundary correspondence. The entanglement spectrum of the postquench state is shown in Fig. 5. When the Chern number $C=2C'_{\mathrm{dyn.}}=2$, the entanglement spectrum has two crossings from $t=0$ to $t=\pi$. On the other hand, when the Chern number is vanishing, the entanglement spectrum does not have crossings.

Since the crossings in the entanglement spectrum are directly related to the topology of the postquench state instead of the postquench order parameter, it is interesting to check the Chern number of the postquench state with vanishing postquench order parameter $\hat{s}=0$. We consider the initial state $|\psi_i\rangle=(0,1,0)^{\mathrm{T}}$ with the initial order parameter $\hat{s}=0$. The postquench state has the form

$$\psi_k(t)=U_k(t)(0,1,0)^{\mathrm{T}}=\begin{pmatrix}-\frac{i}{\sqrt{2}}\sin t(\hat{f}_k-i\hat{g}_k)\\ \cos t\\ -\frac{i}{\sqrt{2}}\sin t(\hat{f}_k+i\hat{g}_k)\end{pmatrix}. \tag{14}$$

The postquench order parameter remains a null vector and the Chern number of the postquench state is zero.

B. 2+1 dimensions

In (2+1)-dimensional cases, the normalized Hamiltonian can be described as $\mathcal{H}_{\mathbf{k}}=\hat{d}_{\mathbf{k}}\cdot\mathbf{S}$, where the unit vector $\hat{d}_{\mathbf{k}}=(\hat{f}_{\mathbf{k}},\hat{g}_{\mathbf{k}},\hat{h}_{\mathbf{k}})$ characterizes the topology of the static Hamiltonian. The postquench state is

$$\begin{aligned}&|\psi(k_1,k_2,t)\rangle\\&=\begin{pmatrix}1+(\cos t-1)\left[1-\frac{1}{2}\left(f_{\mathbf{k}}^2+g_{\mathbf{k}}^2\right)\right]-ih_{\mathbf{k}}\sin t\\ \frac{1}{\sqrt{2}}(f_{\mathbf{k}}+ig_{\mathbf{k}})[h_{\mathbf{k}}(\cos t-1)-i\sin t]\\ \frac{1}{2}(\cos t-1)(f_{\mathbf{k}}+ig_{\mathbf{k}})^2\end{pmatrix}.\end{aligned} \tag{15}$$

The postquench pseudospin is $\hat{s}_{\mathbf{k}}(t)=[f_{\mathbf{k}}h_{\mathbf{k}}(1-\cos t)+g_{\mathbf{k}}\sin t,g_{\mathbf{k}}h_{\mathbf{k}}(1-\cos t)-f_{\mathbf{k}}\sin t,\cos t+h_{\mathbf{k}}^2(1-\cos t)]$ on S^2.

The topology of this postquench pseudospin is characterized by a Hopf fibration $S^3\to S^2$. To compute the Hopf number, we first consider a mapping of the postquench pseudospin from S^2 to S^3. Then the combined mapping from the momentum-time space T^3 to S^3 is characterized by $\pi_3(S^3)$ and can be indexed by the three-dimensional winding number, i.e., the Hopf number can be computed from the three-dimensional winding number. The mapping is $\hat{s}_{\mathbf{k}}\to(\eta_{\uparrow\mathbf{k}},\eta_{\downarrow\mathbf{k}})$, with $\eta_{\uparrow\mathbf{k}}$ and $\eta_{\downarrow\mathbf{k}}$ being two complex numbers satisfying $|\eta_{\uparrow\mathbf{k}}|^2+|\eta_{\downarrow\mathbf{k}}|^2=1$:

$$s_{\mathbf{k}x}+is_{\mathbf{k}y}=2\eta_{\uparrow\mathbf{k}}\bar{\eta}_{\downarrow\mathbf{k}},\quad s_{\mathbf{k}z}=|\eta_{\uparrow\mathbf{k}}|^2-|\eta_{\downarrow\mathbf{k}}|^2. \tag{16}$$

This maps S^2 to S^3. Defining $\eta_{\uparrow\mathbf{k}}=n_1+in_2$ and $\eta_{\downarrow\mathbf{k}}=n_3+in_4$, we have $(n_1,n_2,n_3,n_4)=(\cos\frac{t}{2},h_{\mathbf{k}}\sin\frac{t}{2},g_{\mathbf{k}}\sin\frac{t}{2},f_{\mathbf{k}}\sin\frac{t}{2})$.

The Hopf number can be computed from the mapping $T^3\to S^3\to S^2$ [see Fig. 6] by

$$\begin{aligned}\chi&=\frac{1}{2\pi^2}\int_0^{2\pi}dt\int_{\mathrm{BZ}}d^2k\epsilon_{\mu\nu\rho\tau}n_\mu\partial_{k_x}n_\nu\partial_{k_y}n_\rho\partial_t n_\tau\\&=\frac{1}{4\pi^2}\int_0^{2\pi}dt\sin^2\frac{t}{2}\int_{\mathrm{BZ}}d^2k\hat{d}\cdot\left(\partial_{k_x}\hat{d}\times\partial_{k_y}\hat{d}\right)\\&=\frac{1}{4\pi}\int_{\mathrm{BZ}}d^2k\hat{d}_{\mathbf{k}}\cdot\left(\partial_{k_x}\hat{d}_{\mathbf{k}}\times\partial_{k_y}\hat{d}_{\mathbf{k}}\right)\\&=C.\end{aligned} \tag{17}$$

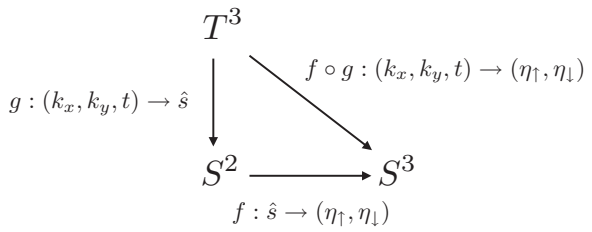

FIG. 6. A combined mapping from the momentum-time torus to $(\eta_\uparrow,\eta_\downarrow)$. This mapping can be characterized by the three-dimensional winding number in Eq. (17).

Here $C=\frac{1}{4\pi}\int d^2k\hat{d}\cdot(\partial_{k_x}\hat{d}\times\partial_{k_y}\hat{d})$ is the Chern number characterizing the static Hamiltonian. Hence we demonstrate the relation between the Hopf number of the postquench pseudospin and the Chern number of the static Hamiltonian $\mathcal{H}_\mathbf{k}=\hat{d}_\mathbf{k}\cdot\mathbf{S}$ by $\chi=C$.

The static Hamiltonian of the spin-1 models with nonvanishing Chern number has been discussed in Ref. [38]. Here we consider the static Hamiltonian with

$$\begin{aligned}\hat{f}_\mathbf{k}&=\frac{t_1\sin k_x}{\sqrt{t_1^2(\sin^2k_x+\sin^2k_y)+(M+\cos k_x+\cos k_y)^2}},\\ \hat{g}_\mathbf{k}&=\frac{t_1\sin k_y}{\sqrt{t_1^2(\sin^2k_x+\sin^2k_y)+(M+\cos k_x+\cos k_y)^2}},\\ \hat{h}_\mathbf{k}&=\frac{M+\cos k_x+\cos k_y}{\sqrt{t_1^2(\sin^2k_x+\sin^2k_y)+(M+\cos k_x+\cos k_y)^2}}.\end{aligned}\tag{18}$$

The Hopf number $|\chi|=1$ when $0<|M/t_1|<2$ and $\chi=0$ otherwise.

Similar to two-band models, the consequence of nonvanishing Hopf number can lead to the crossings of midgap states in the entanglement spectrum. However, the number of midgap states is not directly related to the Hopf number [24]. Unlike the two-band models, the entanglement spectrum of the postquench states in the spin-1 models for a real-space bipartition does not show any crossings. However, if we consider a frequency space bipartition, the entanglement spectrum as a function of (k_x,k_y) has midgap states forming two rings for $|\chi|=1$ and is fully gapped for $\chi=0$, as shown in Fig. 7. These rings are similar to the boundary Fermi rings in Hopf insulators in Refs. [22–24].

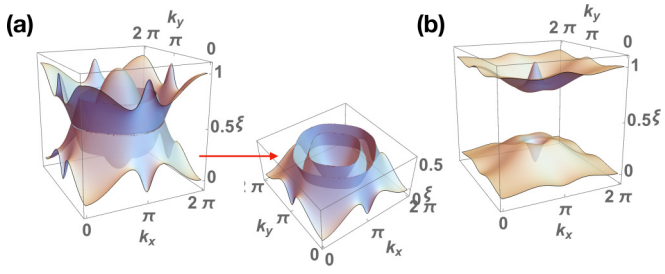

FIG. 7. Entanglement spectrum $\xi(k_x,k_y)$ computed from the postquench state defined in Eq. (15) for frequency space bipartition with (a) $(t_1,M)=(1,0.5)$, (b) $(t_1,M)=(1,2.5)$. The right panel in (a) shows the crossings between the levels are two rings.

V. FOUR-BAND MODELS IN 3+1 DIMENSIONS

Let us consider a four-band model in three dimensions with the following form:

$$\mathcal{H}_\mathbf{k}=f_\mathbf{k}\tau_x+g_\mathbf{k}\tau_y+n_\mathbf{k}\tau_z\sigma_x+m_\mathbf{k}\tau_z\sigma_y,\tag{19}$$

where $\{\sigma_i\}$ and $\{\tau_j\}$ are two sets of Pauli matrices. There are two twofold-degenerate energies $E_\mathbf{k}=\pm\sqrt{f_\mathbf{k}^2+g_\mathbf{k}^2+n_\mathbf{k}^2+m_\mathbf{k}^2}$. The unit vector $\hat{d}_\mathbf{k}=(f_\mathbf{k},g_\mathbf{k},n_\mathbf{k},m_\mathbf{k})/|E_\mathbf{k}|$ characterizes the topology of the static Hamiltonian. Since this unit vector corresponds to a three-sphere S^3, the classification of the static Hamiltonian in three dimensions is the third homotopy group $\pi_3(S^3)=\mathbb{Z}$. The associate topological invariant is the three-dimensional winding number

$$\nu_3=\frac{1}{2\pi^2}\int_{\mathrm{BZ}}d^3k\epsilon^{abcd}\hat{d}_a\partial_{k_x}\hat{d}_b\partial_{k_y}\hat{d}_c\partial_{k_z}\hat{d}_d.\tag{20}$$

The postquench state is evolved by the evolution operator $U_\mathbf{k}(t)=e^{-i\mathcal{H}_\mathbf{k}t}=\cos(|E_\mathbf{k}|t)-i\mathcal{H}_\mathbf{k}\sin(|E_\mathbf{k}|t)$. It will recur to the initial state at $t=2\pi/|E_\mathbf{k}|$. For simplicity, we normalize the Hamiltonian $|E_\mathbf{k}|=1$ in the following discussion.

To have nontrivial topology of the postquench order parameter in $3+1$ dimensions, the manifold of the postquench order parameter can be a four-sphere S^4 such that $\pi_4(S^4)=\mathbb{Z}$. We consider the initial state $|\psi_i\rangle=(1,0,0,0)^\mathrm{T}$. The corresponding postquench state is

$$|\psi_\mathbf{k}(t)\rangle=\begin{pmatrix}\cos t\\ -i\sin t(n_\mathbf{k}+im_\mathbf{k})\\ -i\sin t(f_\mathbf{k}+ig_\mathbf{k})\\ 0\end{pmatrix}\tag{21}$$

and a postquench order parameter can be defined as

$$\begin{aligned}\mathbf{L}&=\langle\psi_\mathbf{k}(t)|(\tau_x,\tau_y,\tau_z\sigma_x,\tau_z\sigma_y,\tau_z\sigma_z)|\psi_\mathbf{k}(t)\rangle\\ &=(\hat{g}_\mathbf{k}\sin2t,-\hat{f}_\mathbf{k}\sin2t,\hat{n}_\mathbf{k}\sin2t,-\hat{m}_\mathbf{k}\sin2t,\cos2t),\end{aligned}\tag{22}$$

such that $|\mathbf{L}|=1$, i.e., the manifold for this postquench order parameter is a four-sphere S^4. The topology of the postquench order parameter can be indexed by the second Chern number

$$\begin{aligned}C_2&=\frac{-3}{8\pi^2}\int_0^{\pi/2}dt\int_{\mathrm{BZ}}d^3k\epsilon^{abcde}L_a\partial_{k_x}L_b\partial_{k_y}L_c\partial_{k_z}L_d\partial_tL_e\\ &=\frac{3}{4\pi^2}\int_0^{\pi/2}\sin^3(2t)\int_{\mathrm{BZ}}d^3k\epsilon^{abcd}\hat{d}_a\partial_{k_x}\hat{d}_b\partial_{k_y}\hat{d}_c\partial_{k_z}\hat{d}_d\\ &=\nu_3.\end{aligned}\tag{23}$$

Here we demonstrate that the second Chern number of the postquench order parameter is equal to the three-dimensional winding number of the static Hamiltonian. Notice that the period of the postquench order parameter is π and there is an intrinsic symmetry,

$$\begin{aligned}&L_a(t)\partial_{k_x}L_b(t)\partial_{k_y}L_c(t)\partial_{k_z}L_d(t)\partial_tL_e(t)\\ &\quad=L_a(-t)\partial_{k_x}L_b(-t)\partial_{k_y}L_c(-t)\partial_{k_z}L_d(-t)\partial_tL_e(-t).\end{aligned}\tag{24}$$

To have a nonvanishing second Chern number, the time integral is taking from 0 to $\pi/2$.

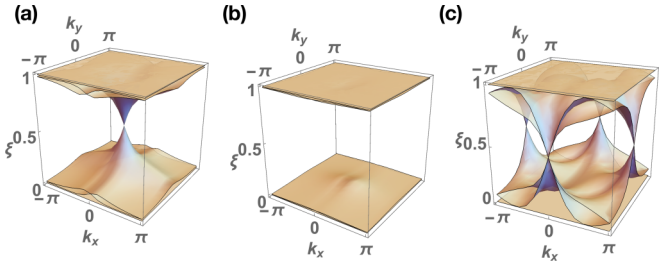

FIG. 8. Entanglement spectrum $\xi(k_y,k_z)$ computed from the postquench state defined in Eq. (21) for a real-space bipartition at $t=\pi/2$ with (a) $M=2$, (b) $M=4$, and (c) $M=0$, where M is the parameter in Eq. (25).

To demonstrate the relation between the nonvanishing second Chern number and the entanglement spectrum of the postquench state, we consider the functions in the static Hamiltonian in Eq. (19) being

$$f_{\mathbf{k}}=\sin k_x,\quad g_{\mathbf{k}}=\sin k_y,\quad n_{\mathbf{k}}=\sin k_z,$$
$$m_{\mathbf{k}}=M-\cos k_x-\cos k_y-\cos k_z. \tag{25}$$

The three-dimensional winding number characterizing the static Hamiltonian is

$$\nu_3=\begin{cases}1, & 1<|M|<3,\\ -2, & |M|<1,\\ 0, & 3<|M|.\end{cases}$$

The entanglement spectrum of the postquench state reflects the nontrivial topology of the postquench state. The Berry connection associated with the postquench states are

$$A_t=0,$$
$$A_{k_i}=-\sin^2 t\left(n\partial_{k_i}m-n\partial_{k_i}m+f\partial_{k_i}g-g\partial_{k_i}f\right). \tag{26}$$

We can compute the three-dimensional polarization from the Chern-Simons 3-form of the postquench state,

$$\begin{aligned}P_3&=\frac{-1}{4\pi^2}\int_{\mathrm{BZ}}d^3k\epsilon^{\alpha\beta\gamma}A_\alpha\partial_\beta A_\gamma\\&=\frac{1}{2\pi^2}\sin^4 t\int_{\mathrm{BZ}}d^3k\epsilon^{abcd}\hat{d}_a\partial_{k_x}\hat{d}_b\partial_{k_y}\hat{d}_c\partial_{k_z}\hat{d}_d\\&=\nu_3\sin^4 t.\end{aligned} \tag{27}$$

From the point of view of the dimensional reduction [39,40], the second Chern number can be computed by the three-dimensional polarization

$$C_2=\int_0^{\pi/2}dt\,\partial_t P_3(t)=\nu_3. \tag{28}$$

At $t=\pi/2$, the postquench state describes a three-dimensional topological insulator with the three-dimensional polarization $P_3=C_2$. Hence the nonvanishing second Chern number characterizing the postquench order parameter leads to Dirac-cone-like excitations in the entanglement spectrum of the postquench state for a real-space bipartition. In the case that $C_2=-1$, there is one Dirac cone at $(k_y,k_z,t)=(0,0,\pi/2)$ [Fig. 8(a)]. In the case that $C_2=-2$, there are two Dirac cones at $(k_y,k_z,t)=(0,\pi,\pi/2)$ and $(\pi,0,\pi/2)$ [Fig. 8(c)]. And the entanglement spectrum is fully gapped for $C_2=0$ [Fig. 8(b)]. The number of Dirac cones in the entanglement spectrum is equal to the second Chern number characterizing the postquench order parameter. On the other hand, the Berry connection $A_t=0$ indicates no midgap states in the entanglement Hamiltonian for a frequency space bipartition. Numerically, we observe the entanglement spectrum are fully gapped for either trivial (vanishing second Chern number) or topological (nonvanishing second Chern number) postquench states.

TABLE I. $\mathcal{M}_{\mathcal{H}_{\mathbf{k}}}$ is the manifold of the static Hamiltonian and $\mathcal{M}_{\hat{n}_{\mathbf{k}}(t)}$ is the manifold of the postquench order parameter. The classification based on the homotopy groups gives the topological invariants of the static Hamiltonian in d dimensions and the postquench order parameter in $d+1$ dimensions. These two topological invariants are related.

	$d=1$	$d=2$	$d=3$
$\pi_d(\mathcal{M}_{\mathcal{H}_{\mathbf{k}}})$	$\pi_1(S^1)\to\nu$	$\pi_2(S^2)\to C$	$\pi_3(S^3)\to\nu_3$
$\pi_{d+1}(\mathcal{M}_{\hat{n}_{\mathbf{k}}(t)})$	$\pi_2(S^2)\to C_{\mathrm{dyn.}}$	$\pi_3(S^2)\to\chi$	$\pi_4(S^4)\to C_2$

VI. DISCUSSION

We demonstrate the relation between the topological invariant of the static Hamiltonian in d dimensions and the topological invariant of the postquench order parameter in $d+1$ dimensions by use of homotopy groups. We show that the entanglement spectrum of the postquench state reveals its topological property. If the postquench order parameter has a nonvanishing topological invariant, the entanglement spectrum has midgap states forming Dirac cones or rings. Our results are summarized in Table I.

The thriving developments of cold-atom experiments provide a way to measure the dynamics of the postquench states by the method of Bloch state tomography [41–43]. For example, in a hexagonal optical lattice, one can prepare a localized cold-atom cloud only at one of the sublattices (A sites) and let it evolve by a sudden quench to a Chern insulator. The nonvanishing dynamical Chern number will lead to a momentum-time skyrmion which can be mapped out by the momentum-time–resolved Bloch state tomography. This measurement in principle can be extended to spin-1 models and the four-band models with nontrivial topology in cold-atom systems [44].

Before we close the discussion, we would like to point out some future directions.

(1) It has been proposed theoretically that a measurement protocol to access the entanglement spectrum can be realized in cold-atoms experiments [45]. The midgap states in the entanglement spectrum in principle can be observed in our quench setup.

(2) Up to date, the entanglement property in the frequency space is only discussed in a two-photon state [46–48]. It will be an intriguing task for finding the experimental realization in condensed-matter and cold-atom systems.

(3) Although the directions of time and momentum are both periodic, they are NOT exchangeable in the quench dynamics. This no-exchangeability reflects the property of the entanglement spectrum with different bipartitions in real and frequency spaces.

To understand the condition of the existence of midgap states in the entanglement spectrum, it is desired to study the structure of the reduced density matrix of the postquench state for different bipartitions in real and frequency spaces.

(4) The interaction and disorder effects in the quench dynamics are an interesting direction to study. In the one-dimensional case, it is shown that the disorder does not remove the crossings in the entanglement spectrum under symmetry constraints [13]. It will be interesting to investigate the robustness of midgap states in the entanglement spectrum for higher-dimensional cases.

(5) One possible extension of our analysis is to consider the higher-order homotopy group. With the development of the synthetic dimensions [49–51], our method can generalize to dimensions higher than $3+1$. One interesting model [52] is a six-dimensional four-band model [Eq. (19)] with a postquench order parameter on S^4. The static Hamiltonian can be classified by $\pi_6(S^3)=\mathbb{Z}_{12}$, and the postquench order parameter can be categorized by $\pi_{6+1}(S^4)=\mathbb{Z}\times\mathbb{Z}_{12}$ described by the second Hopf fibration $S^7\to S^4$.

ACKNOWLEDGMENTS

The author would like to thank Natan Andrei, Piers Coleman, Elio König, Yashar Komijani, Xueda Wen, and Bi Zhen for valuable discussions. The author especially thanks Victor Drouin-Touchette for carefully reading the manuscript and helpful comments. This work was supported by a Rutgers Center for Materials Theory group postdoc grant (P.-Y. C.).

[1] T. Kinoshita, T. Wenger, and D. S. Weiss, Nature (London) **440**, 900 (2006).
[2] N. Navon, A. L. Gaunt, R. P. Smith, and Z. Hadzibabic, Nature (London) **539**, 72 (2016).
[3] M. Atala, M. Aidelsburger, J. T. Barreiro, D. Abanin, T. Kitagawa, E. Demler, and I. Bloch, Nat. Phys. **9**, 795 (2013).
[4] M. Aidelsburger, M. Atala, M. Lohse, J. T. Barreiro, B. Paredes, and I. Bloch, Phys. Rev. Lett. **111**, 185301 (2013).
[5] M. Aidelsburger, M. Lohse, C. Schweizer, M. Atala, J. T. Barreiro, S. Nascimbène, N. R. Cooper, I. Bloch, and N. Goldman, Nat. Phys. **11**, 162 (2014).
[6] H. Miyake, G. A. Siviloglou, C. J. Kennedy, W. C. Burton, and W. Ketterle, Phys. Rev. Lett. **111**, 185302 (2013).
[7] G. Jotzu, M. Messer, R. Desbuquois, M. Lebrat, T. Uehlinger, D. Greif, and T. Esslinger, Nature (London) **515**, 237 (2014).
[8] Z. Wu, L. Zhang, W. Sun, X.-T. Xu, B.-Z. Wang, S.-C. Ji, Y. Deng, S. Chen, X.-J. Liu, and J.-W. Pan, Science **354**, 83 (2016).
[9] N. H. Lindner, G. Refael, and V. Galitski, Nat. Phys. **7**, 490 (2011).
[10] L. Jiang, T. Kitagawa, J. Alicea, A. R. Akhmerov, D. Pekker, G. Refael, J. I. Cirac, E. Demler, M. D. Lukin, and P. Zoller, Phys. Rev. Lett. **106**, 220402 (2011).
[11] A. Gómez-León and G. Platero, Phys. Rev. Lett. **110**, 200403 (2013).
[12] C. Yang, L. Li, and S. Chen, Phys. Rev. B **97**, 060304 (2018).
[13] Z. Gong and M. Ueda, arXiv:1710.05289 .
[14] C. Wang, P. Zhang, X. Chen, J. Yu, and H. Zhai, Phys. Rev. Lett. **118**, 185701 (2017).
[15] M. Tarnowski, F. Nur Ünal, N. Fläschner, B. S. Rem, A. Eckardt, K. Sengstock, and C. Weitenberg, arXiv:1709.01046 .
[16] M. S. Foster, M. Dzero, V. Gurarie, and E. A. Yuzbashyan, Phys. Rev. B **88**, 104511 (2013).
[17] M. S. Foster, V. Gurarie, M. Dzero, and E. A. Yuzbashyan, Phys. Rev. Lett. **113**, 076403 (2014).
[18] Y. Liao and M. S. Foster, Phys. Rev. A **92**, 053620 (2015).
[19] A. Bermudez, D. Patanè, L. Amico, and M. A. Martin-Delgado, Phys. Rev. Lett. **102**, 135702 (2009).
[20] A. Bermudez, L. Amico, and M. A. Martin-Delgado, New J. Phys. **12**, 055014 (2010).
[21] Quantum states can be entangled in the frequency domain. One can compute its entanglement property from the frequency space bipartition.
[22] C. Liu, F. Vafa, and C. Xu, Phys. Rev. B **95**, 161116 (2017).
[23] J. E. Moore, Y. Ran, and X.-G. Wen, Phys. Rev. Lett. **101**, 186805 (2008).
[24] D.-L. Deng, S.-T. Wang, C. Shen, and L.-M. Duan, Phys. Rev. B **88**, 201105 (2013).
[25] C.-K. Chiu, J. C. Y. Teo, A. P. Schnyder, and S. Ryu, Rev. Mod. Phys. **88**, 035005 (2016).
[26] A. Kitaev, AIP Conf. Proc. **1134**, 22 (2009).
[27] G. Abramovici and P. Kalugin, Int. J. Geom. Methods Mod. Phys. **09**, 1250023 (2012).
[28] T. Morimoto and A. Furusaki, Phys. Rev. B **88**, 125129 (2013).
[29] G. D. Nittis and K. Gomi, J. Geom. Phys. **86**, 303 (2014).
[30] R. Kennedy and M. R. Zirnbauer, Commun. Math. Phys. **342**, 909 (2016).
[31] T. Bzdušek and M. Sigrist, Phys. Rev. B **96**, 155105 (2017).
[32] I. Peschel, J. Phys. A: Math. Gen. **36**, L205 (2003).
[33] P.-Y. Chang, C. Mudry, and S. Ryu, J. Stat. Mech. (2014) P09014.
[34] F. Wilczek and A. Zee, Phys. Rev. Lett. **51**, 2250 (1983).
[35] R. Barnett, G. R. Boyd, and V. Galitski, Phys. Rev. Lett. **109**, 235308 (2012).
[36] S.-Y. Lee, J.-H. Park, G. Go, and J. H. Han, J. Phys. Soc. Jpn. **84**, 064005 (2015).
[37] T. L. Curtright, D. B. Fairlie, and C. K. Zachos, SIGMA **10**, 084 (2014).
[38] G. Go, J.-H. Park, and J. H. Han, Phys. Rev. B **87**, 155112 (2013).
[39] X.-L. Qi, T. L. Hughes, and S.-C. Zhang, Phys. Rev. B **78**, 195424 (2008).
[40] S. Ryu, A. P. Schnyder, A. Furusaki, and A. W. W. Ludwig, New J. Phys. **12**, 065010 (2010).
[41] E. Alba, X. Fernandez-Gonzalvo, J. Mur-Petit, J. K. Pachos, and J. J. Garcia-Ripoll, Phys. Rev. Lett. **107**, 235301 (2011).
[42] P. Hauke, M. Lewenstein, and A. Eckardt, Phys. Rev. Lett. **113**, 045303 (2014).
[43] N. Fläschner, B. S. Rem, M. Tarnowski, D. Vogel, D.-S. Lühmann, K. Sengstock, and C. Weitenberg, Science **352**, 1091 (2016).

[44] N. R. Cooper, J. Dalibard, and I. B. Spielman, arXiv:1803.00249.
[45] H. Pichler, G. Zhu, A. Seif, P. Zoller, and M. Hafezi, Phys. Rev. X **6**, 041033 (2016).
[46] C. K. Law, I. A. Walmsley, and J. H. Eberly, Phys. Rev. Lett. **84**, 5304 (2000).
[47] M. Kues, C. Reimer, P. Roztocki, L. R. Cortés, S. Sciara, B. Wetzel, Y. Zhang, A. Cino, S. T. Chu, B. E. Little, D. J. Moss, L. Caspani, J. Azaña, and R. Morandotti, Nature (London) **546**, 622 (2017).
[48] H. H. Jen, J. Phys. B **49**, 035503 (2016).
[49] O. Boada, A. Celi, J. I. Latorre, and M. Lewenstein, Phys. Rev. Lett. **108**, 133001 (2012).
[50] A. Celi, P. Massignan, J. Ruseckas, N. Goldman, I. B. Spielman, G. Juzeliūnas, and M. Lewenstein, Phys. Rev. Lett. **112**, 043001 (2014).
[51] H. M. Price, T. Ozawa, and N. Goldman, Phys. Rev. A **95**, 023607 (2017).
[52] P.-Y. Chang (unpublished).